J Fusion Energ (2016) 35:613–620
DOI 10.1007/s10894-016-0086-x

ORIGINAL RESEARCH

A Novel Vacuum System Control Strategy for High Intensity D–T Fusion Neutron Generator

Weitian Wang[1,2] · Yong Song[2] · Jianye Wang[2] · Peng Xu[2] · Lingli Kong[1,2]

Published online: 9 March 2016
© Springer Science+Business Media New York 2016

Abstract High intensity D–T fusion neutron generator (HINEG) is a high voltage accelerator-based D–T fusion neutron facility, which provides a significant platform for nuclear technology researches. The steady operation of HINEG vacuum system is enormously significant for its beam quality. In this paper, in order to eliminate the drawbacks and disadvantages caused by the time delay element in vacuum system, a gain adaptive compensation control strategy was proposed for vacuum system. In accordance with vacuum-pumping mechanism, the vacuum dynamic equilibrium equation was transformed from the time domain to the complex frequency domain by means of Laplace transformation, and the system transfer function in vacuum pumping process was derived. The experimental results analyses showed that the overshoot and settling time are eliminated effectively with this gain adaptive compensation control algorithm, which indicated that the system self-regulation and anti-interference performances were greatly improved.

Keywords Fusion neutron generator · Vacuum system · Control algorithm · Gain adaptive compensation · Transfer function

✉ Yong Song
yong.song@fds.org.cn

Weitian Wang
wwtwang@mail.ustc.edu.cn

[1] University of Science and Technology of China, Hefei 230026, Anhui, China

[2] Key Laboratory of Neutronics and Radiation Safety, Institute of Nuclear Energy Safety Technology, Chinese Academy of Sciences, Hefei 230031, Anhui, China

Introduction

Fusion neutron facility serves as a significant platform for nuclear energy researches [1], including nuclear material and blanket technology [2, 3], reactor physics and engineering design [4–7], radiation medical physics [8], nuclear software and simulation [9–11] and other nuclear technologies, etc. High intensity D–T fusion neutron generator (HINEG) is a high voltage accelerator-based D–T fusion neutron facility [12, 13], its parameters of neutron yield are designed to be the highest in D–T fusion neutron facilities in China, is being constructed by Institute of Nuclear Energy Safety Technology, Chinese Academy of Sciences. HINEG could provide 14 MeV monoenergetic neutron with source intensity of 10^{13} n/s which is generated in deuterium–tritium reaction by bombardment of tritium target. Vacuum system, which is one of the key subsystems in this neutron generator, supplies a collision-free condition for the deuterium ion beam without loss and instability on account of interaction with other atmospheric molecules [14]. In HINEG operation, the beam could keep enough life and high quality to be accumulated as well as accelerated to reach the designed kinetic energy in the vacuum system.

With the objective of maintaining the dynamic equilibrium of vacuum various parameters and ensuring the beam without being damaged, the accurate and steady control strategy with good robustness should be adopted when HINEG is in operation. Due to the vacuum system is a time delay system, when the conventional PID control algorithm is being employed in vacuum-pumping controlling, the controlled parameters present completely unresponsive within the hysteretic time after the control system operation. Consequently, the vacuum system is unable to adjust with the controlled variables to eliminate errors and interferences timely and correctly, which will bring about

serious overshoot and long settling time in the control system. And the overshoot will become larger with the increase of phase lag in controlling process, thus the control system stability is lessened and even serious operational accidents occur. In this paper, on the basis of vacuum-pumping mechanism, the vacuum dynamic equilibrium equation was transformed from the time domain to the complex frequency domain by means of Laplace transformation, and the system transfer function in vacuum pumping process was derived. A gain adaptive compensation control strategy was employed to design the controller to overcome the drawbacks caused by vacuum system hysteresis quality. From the experimental results analyses, it turned out that the system self-regulation and anti-interference performances were well improved with this control algorithm.

Vacuum System Modeling Methodology

System Pumping Equation

The pressure intensity of the vacuum tube becomes weaken when vacuum pumping system starts working, and the actual pressure is determined by a range of gas movements and interactions. These elements are composed of the functions of vacuum pumps, the deflations of different air sources in the system and the interferences outside. As shown in Fig. 1, the gas starts to flow when the pressure difference appears at both ends of the vacuum tube, of which length is L and diameter is D. Once the airstream reaches steady state, the gas flow through the pipeline can be expressed by

$$Q = C(P_1 - P_2) \tag{1}$$

where Q denotes gas flow, C denotes the conductance of vacuum tube, P denotes the pressure intensity inside the vacuum tube [15].

The gas inside the vacuum system is blocked by the tube wall when vacuum pumps coming into operation. For each second, the extracted gas from the tube could weaken the tube pressure, and the tube wall or joint part will result in air leakage at the same time. At any given moment t, the gas increment is formed as

$$V\frac{\mathrm{d}P}{\mathrm{d}t} + \frac{CS_p}{C+S_p}P = V\frac{\mathrm{d}P}{\mathrm{d}t} + S_eP = Q_f + Q_s + Q_z + Q_l \tag{2}$$

where V denotes the volume of the vacuum tube, $\frac{\mathrm{d}P}{\mathrm{d}t}$ denotes the change rate of pressure intensity inside the tube, S_p denotes the pumping speed, S_e denotes the effective pumping speed, Q_f denotes the leakage gas flow, Q_s denotes the permeation gas flow, Q_z denotes the evaporation gas flow, Q_l denotes the others leakage gas flow [15]. We employ Q to denote $Q_f + Q_s + Q_z + Q_l$ when the gas inside vacuum system reaches dynamic equilibrium. Obviously, by Eq. (2), we can obtain the following expression

$$V\frac{\mathrm{d}P}{\mathrm{d}t} + S_eP = Q \tag{3}$$

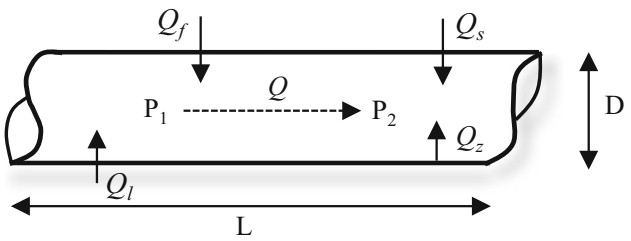

Fig. 1 The vacuum system tube sketch

Transfer Function Model Establishment

With the purpose of designing an accurate and steady controller with good robustness, a special transfer function which could reflect the internal relationships among the parameters of vacuum system operation is required. The vacuum dynamic equilibrium equation is transformed from the time domain to the complex frequency domain by means of Laplace transformation. Firstly, Eq. (3) can be described by the following differential equation

$$\frac{V}{S_e}\frac{\mathrm{d}P}{\mathrm{d}t} + P = \frac{1}{S_e}Q \tag{4}$$

Based on Eq. (4), the Laplace transformation is adopted under zero initial condition, and the pumping down equation can be described by

$$\frac{V}{S_e}P(s)s + P(s) = \frac{1}{S_e}Q(s) \tag{5}$$

where s denotes transformation factor. Furthermore, the transfer function of the vacuum dynamic equilibrium system is expressed as

$$G_1(s) = \frac{P(s)}{Q(s)} = \frac{\frac{1}{S_e}}{\frac{V}{S_e}s + 1} \tag{6}$$

Equation (6) shows the output characteristic of the gas flow varies with tube pressure. However, the vacuum system presents a time delay in actual operation process, that is the gas flow Q or the tube pressure P spends a period of time τ in changing from a certain state to another one. Hence the transfer function is supposed to be calibrated

with a time delay link $e^{-\tau s}$ in practice, and Eq. (6) can be described by

$$G(s) = G_1(s)e^{-\tau s} = \frac{\frac{1}{S_e}}{\frac{V}{S_e}s + 1}e^{-\tau s} \tag{7}$$

where τ denotes the pure delay time. By Eqs. (2) and (7), we can obtain

$$G(s) = \frac{\frac{1}{S_e}}{\frac{V}{S_e}s + 1}e^{-\tau s} = \frac{\frac{C+S_p}{CS_p}}{\frac{(C+S_p)V}{CS_p}s + 1}e^{-\tau s} = \frac{K}{Ts + 1}e^{-\tau s} \tag{8}$$

where $K = \frac{C+S_p}{CS_p}$, $T = \frac{(C+S_p)V}{CS_p}$.

Time Delay Element Effects

For the purpose of analyzing the influence on the control system made by the time delay link in the vacuum system, we set a given vacuum tube of which length $L = 2$ m and diameter $D = 140$ mm, the pumping speed $S_p = 1.2$ m^3/s. Based on Eq. (8), the transfer function is formed as

$$G(s) = \frac{6.86}{0.21s + 1}e^{-\tau s} \tag{9}$$

The stability of the control system obtained from Eq. (9) changes correspondingly when the delay time τ is varying. Figure 2 presents the step responses of open-loop transfer function and the Nyquist curves [16] of the control system under $\tau = 0, 0.5, 1$ s and 1.5 s, respectively. As shown in Fig. 2, along with the increase of delay time, the settling time becomes longer accordingly and the system hysteresis is more and more serious. Moreover, the number of turns of the coordinate point $(-1,0)$ surrounded by the Nyquist curve increase as well, which indicates that the system stability is getting worse. Therefore, eliminating the hysteresis to improve the qualities of control system is the key work in the controller design and implementation.

Firstly, the conventional PID control algorithm is adopted to design the vacuum system controller. Figure 3a shows the bode plot [17] of the open-loop system when $\tau = 0.02$ s, we can get that the phase cross-over frequency $w_g = 81.6$ rad/s and the magnitude margin $L_h = 7.96$ dB from the partial enlarged view as presented in Fig. 3b.

The stable boundary law is employed here in this PID controller parameters setting. After being adjusted, the controller is formed as

$$G_c = 1.53 + \frac{5}{s} + 0.01s \tag{10}$$

The random noise interference [18] of which magnitude range from -0.1 to 0.1 is imported in the system commissioning. From the system step response by input $r_1 = r_0 \pm 0.1$, as shown in Fig. 4, the overshoot and settling time are too large to weaken the system anti-interference performances, which are likely to be able to result in system instability and operation accident.

Control Strategy Design and Application

Gain Adaptive Compensation Control Algorithm

Gain adaptive compensation control algorithm is an optimized and improved strategy based on the Smith predictive compensation [19] controller, which is added with a divider, a multiplier and a lead link. During the system operation, a correcting signal used for calibrating the predictor gain to vary with the object gain is produced by the ratio of compensation model to system output in accordance with the gain adaptive compensation control mechanism. Afterwards, the PID control algorithm is employed based on the gain compensation. Figure 5 presents the operating principle of gain adaptive compensation control algorithm.

After the time delay compensation model is being introduced, as indicated in Fig. 5, the mathematical model of the generalized adjustment object in this system can be expressed as

$$\begin{aligned} G_g(s) = \frac{M(s)}{U(s)} &= \left[1 + \frac{F(s)}{U(s)}\right]K_pG_p(s)e^{-(\tau_0-\tau_1)s}(1 + \tau_2 s) \\ &= K_vG_p(s)e^{-(\tau_0-\tau_1)s}(1 + \tau_2 s) \end{aligned} \tag{11}$$

where $K_v = [1 + \frac{F(s)}{U(s)}]K_p$.

The time delay effects can be compensated absolutely when $\tau_0 - \tau_1 = 0$ according to the expression of Eq. (11), hence the stability of the regulating system is unaffected by the deviations between K_q and K_p. With regard to the interference signal $F(s)$, from Eq. (11), the combination $[1 + \frac{F(s)}{U(s)}]K_p$ can be represented as an alterable gain K_v, which presents the adaptive ability possessed in the control model operation. Additionally, the expansion of delay link can be described as

$$e^{-(\tau_0-\tau_1)s} = \frac{1}{1 + (\tau_0 - \tau_1)s + \frac{(\tau_0-\tau_1)^2s^2}{2} + \frac{(\tau_0-\tau_1)^3s^3}{6} + \cdots + \frac{(\tau_0-\tau_1)^ns^n}{n!}} \tag{12}$$

When $\tau_0 - \tau_1 \to 0$,

$$e^{-(\tau_0-\tau_1)s} \approx \frac{1}{1 + (\tau_0 - \tau_1)s} \tag{13}$$

Hence Eq. (11) can be formed as

$$G_g(s) = K_vG_p(s)\frac{1 + \tau_2 s}{1 + (\tau_0 - \tau_1)s} \tag{14}$$

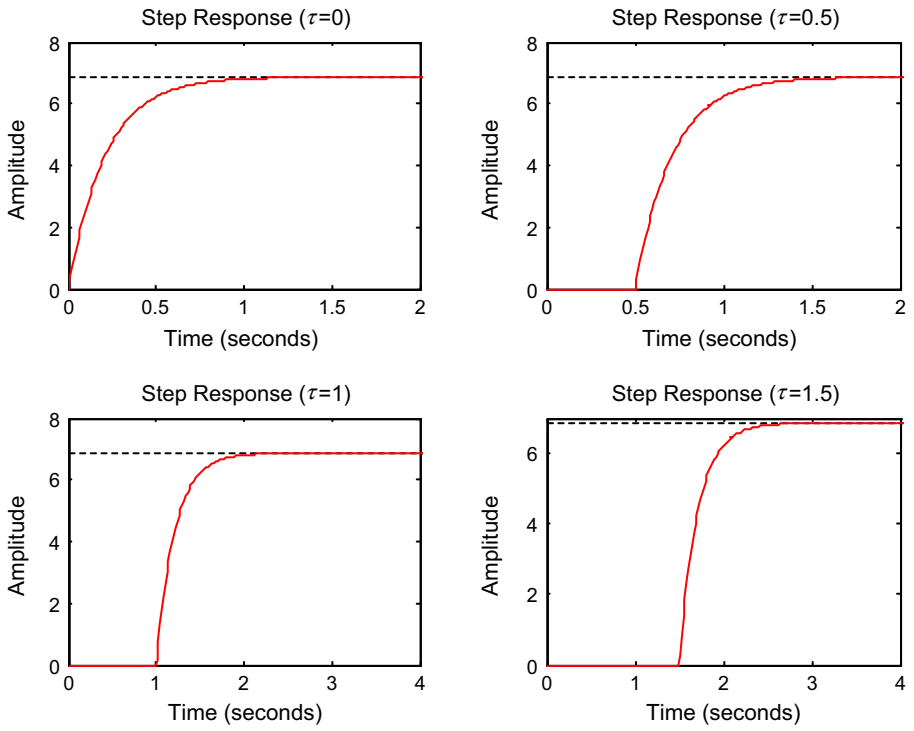

(a) Step responses

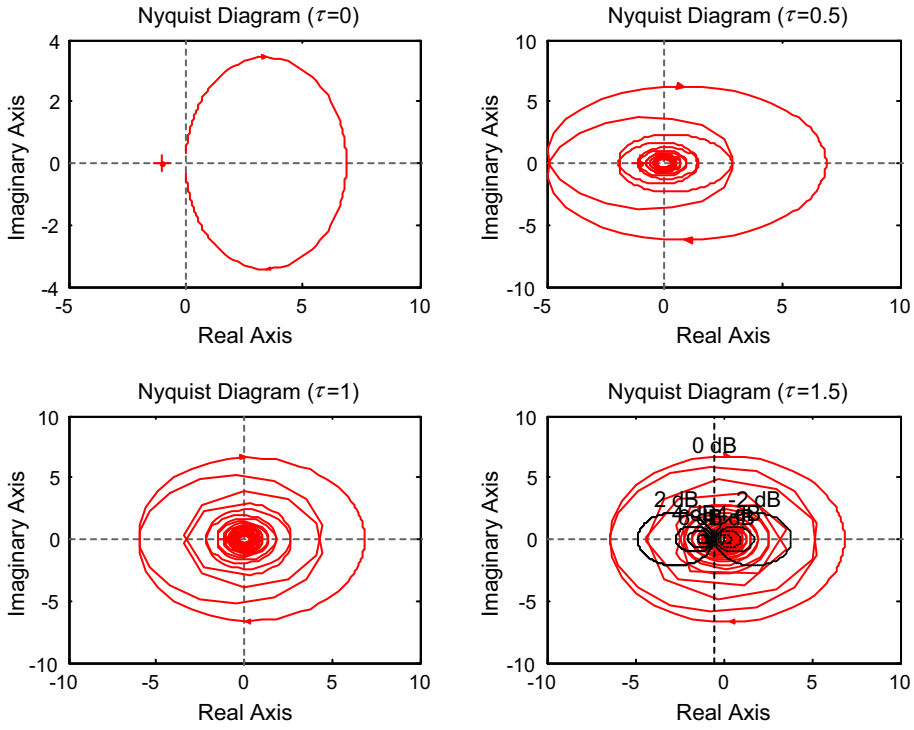

(b) Nyquist curves

Fig. 2 The variation of the system step responses and Nyquist curves with delay time. **a** Step responses, **b** Nyquist curves

Obviously, due to a lead link is brought in, the adaptive ability is shown by compensation model when $\tau_2 = \tau_0 - \tau_1$. And $G_g(s)$ is equal to $K_v G_p(s)$ by this time, the controlled object corresponds to an inertial element, which indicates that the time delay effects are eliminated in system operation.

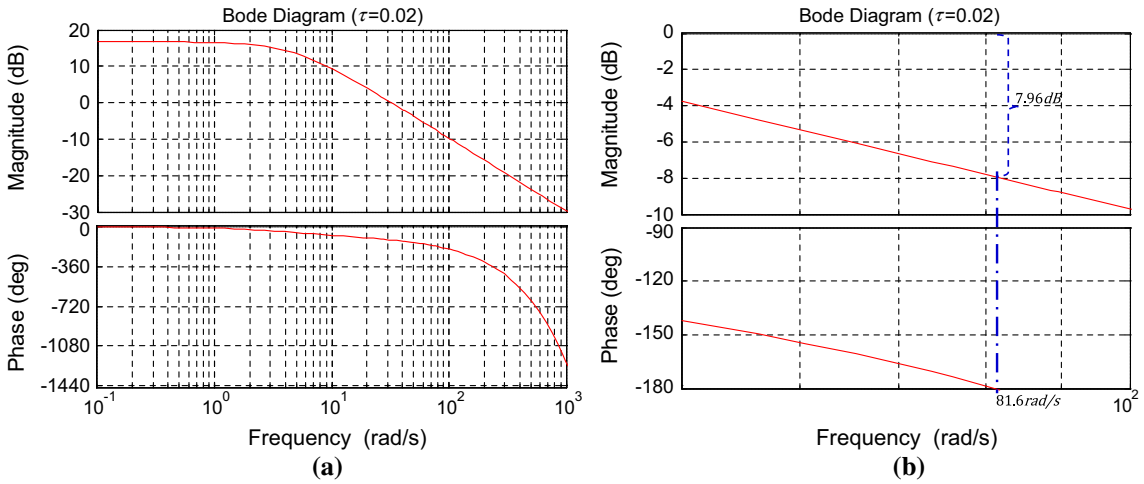

Fig. 3 The bode plot of the open-loop system ($\tau = 0.02$s)

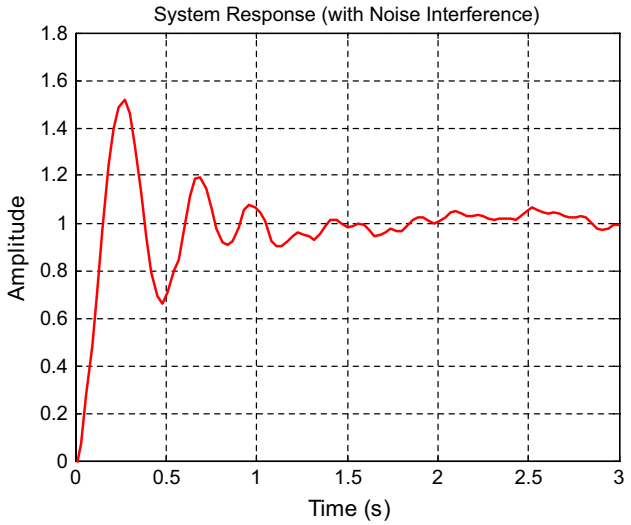

Fig. 4 The system step response with PID controller

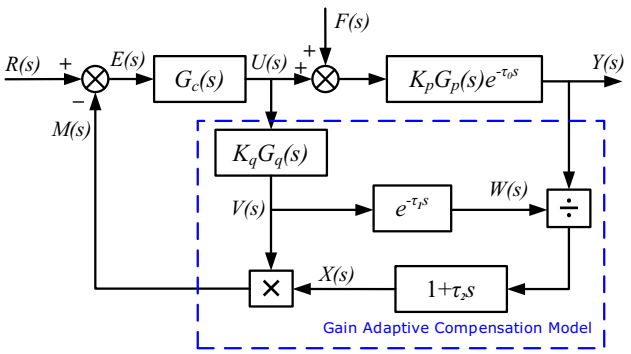

Fig. 5 The gain adaptive compensation control algorithm

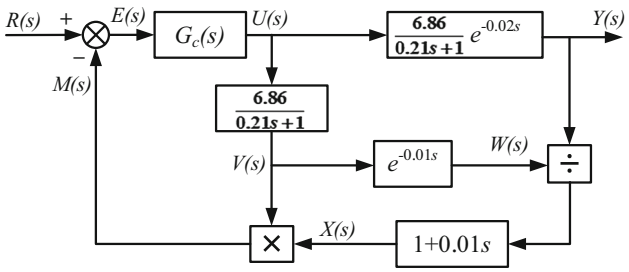

Fig. 6 Modification of the vacuum controller

Vacuum Controller Modification

On the basis of the gain adaptive compensation control algorithm proposed above, the vacuum system controller is improved with the compensation model. The correcting control strategy is present in Fig. 6.

In accordance with Eq. (14), the modified generalized adjustment object is described as

$$G_g(s) = \frac{6.86}{0.21s + 1} \tag{15}$$

Figure 7 shows the Bode plot of the open-loop system without being adjusted after compensation, it can be obtained from the curve that the magnitude margin is an infinite value and the phase margin is 81.6°.

Experimental Results and Analyses

Experimental Testing

Figure 8 presents the hardware architecture of the testing platform. Distributed control technology is employed in

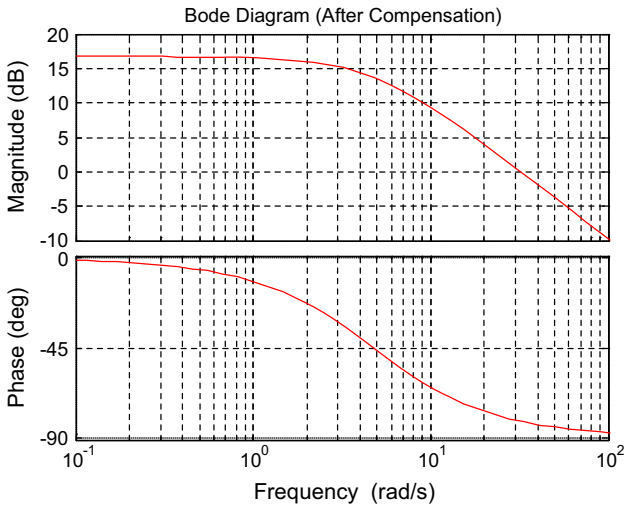

Fig. 7 The Bode plot of the open-loop system after compensating

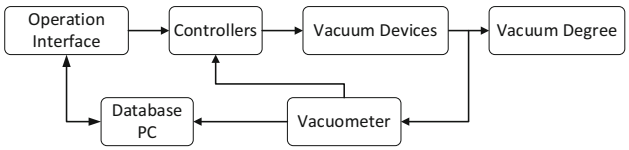

Fig. 8 The hardware architecture of the testing platform

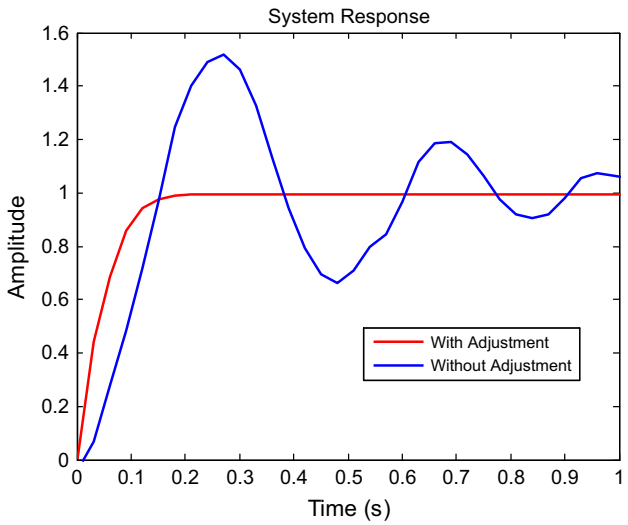

Fig. 9 The system step response after adjustment

this control system hardware configuration and the platform consists of supervision level, controller and vacuum devices. The operation interface runs on the industry computers (IPC) and servers to monitor all the equipment of the platform. All the controlling equipment and filed devices are connected with each other through an intranet

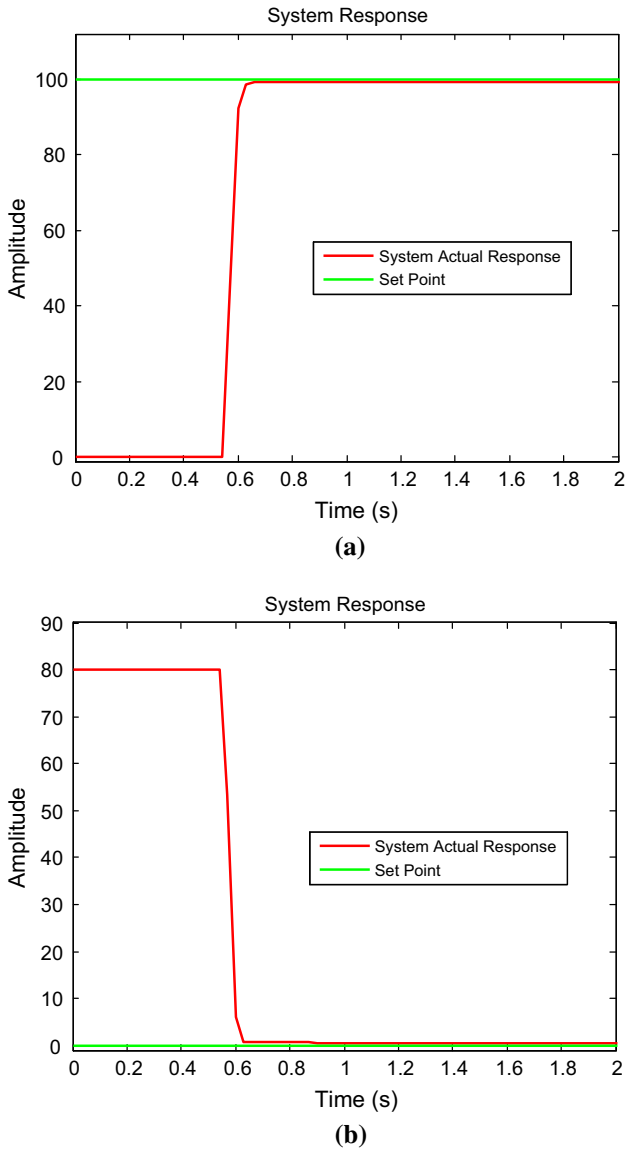

Fig. 10 The system actual response under two different operating conditions. **a** Increase the input value from 0 to 100, **b** decrease the input value from 80 to 0

for communication. The database PC is used for storing testing data during the platform operation for analyses.

When the PID controller is being designed, the parameters of proportional gain K_p, integral factor K_I and differential quotient K_D need to be tuned to meet the control system performances requirements. The trial-and-error pricing [20] is employed for the PID control parameters tuning. By gradually adjustment, the static error and overshoot are close to zero and the system stability is improved vastly when $K_p = 18$ and $K_I = 7.28$. Therefore

$$G_c = 18 + \frac{7.28}{s} \tag{16}$$

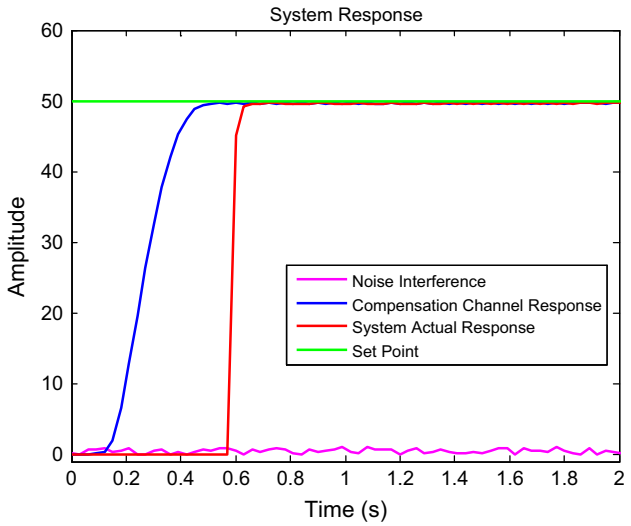

Fig. 11 The system response with gain adaptive compensation control algorithm

Results and Analyses

On the basis of Eq. (16), we obtain the system step response after adjustment, as shown the red solid line in Fig. 9. The picture indicates that the overshoot and settling time of the system are eliminated after been tuned, which increase the system stability effectively.

As shown in Fig. 10, the control algorithm is tested under two different operating conditions, one is increasing the input value from 0 to 100, and another is decrease the input value from 80 to 0. From the picture, It can be obtained that the system actual response is in conformity with the set point well.

The random noise interference of which magnitude range from −0.1 to 1 is imported in the system commissioning with PID controller. The system output response with the gain adaptive compensation control algorithm being employed is presented in Fig. 11, in which the input value is set to 50. The picture presents that, even though interfered by the random noise, the system response is consistent with the input well and the compensation channel response is extremely close to the actual response. As shown by the blue solid line and red solid line in Fig. 11, the settling time of the system actual response and compensation channel response is shortened. Therefore, the drawbacks and disadvantages caused by the time delay element are eliminated, furthermore, the system stability and accuracy are improved greatly.

Conclusion

The steady operation of vacuum system is exceedingly significant for HINEG beam quality. Due to the vacuum system belongs to time delay systems, when the conventional PID control algorithm is adopted in the control system, the response is unable to adjust with the controlled variables to eliminate errors and interferences timely and correctly, which will cause serious overshoot and long settling time. With the purpose of overcoming the drawbacks brought about by vacuum system hysteresis quality, a gain adaptive compensation control strategy was employed in this paper. The experimental results and analyses presented that the anti-interference performances and the system self-regulation were well improved with this control strategy.

Acknowledgments This work is supported by the ITER 973 Program (No. 2014GB112001) and the Strategic Priority Research Program of the Chinese Academy of Sciences (No. XDA03040000). We would further like to thank the great help from the other members of FDS Team in this research.

References

1. J. Pivarč et al., Vacuum system of the multipurpose 14 MeV neutron source in Bratislava: design and status. Vacuum **36**, 527–529 (1986)
2. Y. Wu, F.D.S. Team, Design analysis of the China dual-functional lithium lead (DFLL) test blanket module in ITER. Fusion Eng Des **82**, 1893–1903 (2007)
3. Y. Wu, Design status and development strategy of China liquid lithium-lead blankets and related material technology. J Nucl Mater **367**, 1410–1415 (2007)
4. Y. Wu et al., A fusion-driven subcritical system concept based on viable technologies. Nucl Fusion **51**, 1030–1036 (2011)
5. Y. Wu, F.D.S. Team, Conceptual design activities of FDS series fusion power plants in China. Fusion Eng Des **81**, 2713–2718 (2006)
6. Y. Wu, et al., Development strategy and conceptual design of China Lead-based Research Reactor. Ann Nucl Energy **87**, 511–516 (2016)
7. Y. Wu, Conceptual design and testing strategy of a dual functional lithium-lead test blanket module in ITER and EAST. Nucl Fusion **47**, 1533–1539 (2007)
8. Y. Wu et al., Development of accurate/advanced radiotherapy treatment planning and quality assurance system (ARTS). Chin. Phys. C **32**, 177–182 (2008)
9. Y. Wu et al., CAD-based Monte Carlo program for integrated simulation of nuclear system SuperMC. Ann. Nucl. Energy **82**, 161–168 (2015)
10. Y. Wu et al., A discrete ordinates nodal method for one-dimensional neutron transport calculation in curvilinear geometries. Nucl. Sci. Eng. **133**, 350–357 (1999)
11. Y. Wu, F.D.S. Team, CAD-based interface programs for fusion neutron transport simulation. Fusion Eng. Des. **84**, 1987–1992 (2009)
12. W. Wang et al., Spectrum analyses and diagnoses of 350 kV HVPS ripples on high intensity D–T fusion neutron generator. J. Fusion Energ. **34**, 989–994 (2015)
13. W. Wang et al., Design of the personnel radiation safety interlock system for high intensity D–T fusion neutron generator. J. Fusion Energ. **34**, 346–351 (2015)
14. D. Schmied, Vacuum control and operation of the ESRF accelerator system. Vacuum **60**, 123–129 (2001)
15. Y. Wang, *Vacuum Technology* (Sichuan Publishing House of Science and Technology, Sichuan, 1985), pp. 243–252
16. F. Golnaraghi, B. Kuo, Automatic control systems. Complex Variables **2**, 426–440 (2009)

17. L.H. Keel, S.P. Bhattacharyya, A Bode plot characterization of all stabilizing controllers. Autom. Control IEEE Trans. **55**, 2650–2654 (2010)
18. Lam QM, Stamatakos N, Woodruff C, Ashton S. Gyro modeling and estimation of its random noise sources, in *AIAA Guidance, Navigation, and Control Conference and Exhibit* (AIAA Inc. Texas, USA, 2003)
19. J. Normey-Rico, C. Bordons, E. Camacho, Improving the robustness of dead-time compensating PI controllers. Control Eng. Pract. **5**, 801–810 (1997)
20. Omatu S, Fujinaka T, Yoshioka M. Neuro-PID control for inverted single and double pendulums, in *Systems, Man, and Cybernetics, 2000 IEEE International Conference on* (IEEE, 2000), pp. 2685–2690